metadata, citation and similar papers at core.ac.uk

Accepted Manuscript

Title: The influence of pH on the corrosion rate of high-purity Mg, AZ91 and ZE41 in bicarbonate buffered Hanks' solution

Author: Sean Johnston Zhiming Shi Andrej Atrens

PII: S0010-938X(15)30092-5
DOI: http://dx.doi.org/doi:10.1016/j.corsci.2015.09.018
Reference: CS 6489

To appear in:

Received date: 2-6-2015
Revised date: 18-9-2015
Accepted date: 19-9-2015

Please cite this article as: Sean Johnston, Zhiming Shi, Andrej Atrens, The influence of pH on the corrosion rate of high-purity Mg, AZ91 and ZE41 in bicarbonate buffered Hanks' solution, Corrosion Science http://dx.doi.org/10.1016/j.corsci.2015.09.018

This is a PDF file of an unedited manuscript that has been accepted for publication. As a service to our customers we are providing this early version of the manuscript. The manuscript will undergo copyediting, typesetting, and review of the resulting proof before it is published in its final form. Please note that during the production process errors may be discovered which could affect the content, and all legal disclaimers that apply to the journal pertain.

ACCEPTED MANUSCRIPT

The influence of pH on the corrosion rate of high-purity Mg, AZ91 and ZE41 in bicarbonate buffered Hanks' solution

Sean Johnston[1], Zhiming Shi[1, 2] Andrej Atrens[1,*]

1 The University of Queensland, Materials Engineering, School of Mechanical and Mining Engineering, Brisbane, Qld 4072, Australia

2 The University of Queensland, Centre for Advanced Materials Processing and Manufacturing (AMPAM), Brisbane, Qld 4072, Australia

*Corresponding Author, Andrejs.Atrens@uq.edu.au, +61 7 3365 3748

ACCEPTED MANUSCRIPT

Highlights

Corrosion of high purity (HP) Mg, AZ91 and ZE41, was studied in CO_2-bicarbonate buffered Hanks solution

Corrosion rates were in the following decreasing order: ZE41 > HP Mg > AZ91.

All corrosion rates decreased slightly with increasing pH, attributed to more stable protective films.

A slow fluid flow caused a slightly higher corrosion rate and a more-uniform corrosion morphology

ACCEPTED MANUSCRIPT

Abstract

Corrosion of high purity (HP) Mg, AZ91 and ZE41, was studied in CO_2-bicarbonate buffered Hanks' solution, using mass loss and hydrogen evolution. Corrosion rates were in the following decreasing order: ZE41 > HP Mg > AZ91. Corrosion rates of ZE41 were much higher than those of the other Mg alloys. HP Mg and AZ91 had comparable corrosion rates, but HP Mg corroded more quickly. All corrosion rates decreased slightly with increasing pH, attributed to more stable protective films. A slow fluid flow caused a slightly higher corrosion rate and a more-uniform corrosion morphology for all Mg alloys.

Keywords: A. Magnesium, B. Weight Loss, B. SEM.

ACCEPTED MANUSCRIPT

1.0 Introduction

1.1 Biodegradable magnesium

Biodegradable magnesium (Mg) implants have gathered much interest as an alternative to permanent medical implants, particularly in the fields of cardiovascular and orthopaedic surgery [1-47].

A central issue with magnesium alloys for biodegradable implants is to understand the corrosion behaviour of the magnesium alloys in sufficient detail to be able to confidently predict their behaviour in the body, i.e. *in vivo*. Initial studies by Witte et al. [1, 45, 46] and Staiger et al. [48] indicated that there was little relationship between corrosion behaviour *in vitro* and the behaviour *in vivo*. Zainal Abidin et al. [2] indicated that this was similar to the classic problem of determining long-term service behaviour from short-term laboratory tests. It is only possible to predict long-term service behaviour if the corrosion mechanism in the short-term laboratory tests is the same as in the long-term service behaviour. It is necessary for the *in vitro* tests to be carried out in a solution that produces corrosion similar to that *in vivo*. Zainal Abidin et al. [2] showed that when short-term tests were selected based on this similarity principle, there was good correspondence between *in vitro* corrosion rates and *in vivo* corrosion rates. Zainal Abidin et al. [4] showed that Nor's solution was a good starting solution to predict *in vivo* corrosion behaviour. Nor's solution is Hanks' solution through which CO_2 is bubbled at the appropriate partial pressure, so that the pH is maintained at the physiological pH value by the same buffer system as in blood (CO_2 interacting with bicarbonate ions). Furthermore, Nor's solution has a concentration of the inorganic ions, particularly the corrosive chloride ions, similar to that of blood. Walker et al. [49] used a similar approach, and also showed a good relationship between *in vitro* tests and *in vivo* behaviour.

We have been exploring individually the components of Nor's solution to understand their contribution to the corrosion behaviour. The influence of the chloride ion concentration was studied by Taltavull et al. [50] using high-purity Mg (HP Mg), AZ91 and ZE41. The governing factors were (i) the surface layer formed and its protective properties, (ii) the micro-galvanic coupling between constituent phases in the Mg alloys, and (iii) the morphology of the corrosion.

ACCEPTED MANUSCRIPT

The present research aims to explore (i) the influence of pH using the same alloys (HP Mg, AZ91 and ZE41), and (ii) the influence of flow.

HP Mg, AZ91 and ZE41 were used in this research, not because they are particular candidates for biomedical use, but because they are typical Mg alloys. HP Mg typically has the lowest corrosion rate for Mg alloys. Mg alloys typically consist of two or more phases and the second phases typically accelerate the corrosion of the Mg matrix by micro-galvanic coupling. AZ91 is the most popular Al-containing Mg casting alloy. ZE41 is a typical representative of a commercial Mg alloy containing rare earth elements. The biocompatibility of AZ91 and ZE41 is beyond the scope of this research, nevertheless, biocompatibility of Mg alloys has received much attention [51, 52].

1.2 Influence of pH

The human body maintains the pH at a relatively constant value between 7.35 to 7.45 [53, 54]. However, some pH fluctuations in the body may be possible. During exercise, the metabolism of glucose causes the release of hydrogen ions [55], which would tend to decrease the blood pH. This decrease is compensated by the repository buffer system. There has also been evidence that the pH of a bone fracture site be as low as 5.5 in the period immediately after implantation [56].

The overall corrosion reaction for magnesium, including in a biomedical environment, is given by [1-5, 57]:

$$Mg + 2\,H_2O \rightarrow Mg^{2+} + 2OH^- + H_2 \rightarrow Mg(OH)_2 + H_2 \quad (1)$$

Eq. (1) indicates that it is possible to evaluate the corrosion rate from the volume of hydrogen evolved. This is indeed a common method [2-5, 57]. Typically, the corroding specimen is located within an upturned filter funnel, which channels the evolving hydrogen into an upturned burette, as illustrated in Fig. 1. This means that the corrosion conditions for such a corroding specimen are stagnant, and the corrosion behaviour might be somewhat different to a specimen just exposed to the solution such as the specimen in the left hand tank in Fig. 1.

Several previous studies have considered the influence of pH on the biocorrosion of Mg alloys. However key issues in the experimental procedures warrant further consideration of this topic. Xin et al. [58] found that the pH increase associated with increased OH^-

ACCEPTED MANUSCRIPT

concentration in simulated body fluid caused precipitation of magnesium phosphate and carbonate, stabilized magnesium hydroxide, and decreased the corrosion rate of AZ91. The decreased corrosion rate was attributed to the increased stability and thickness of the surface corrosion-product layers [58]. Ng et al. [57] found that the biocorrosion in Hanks' solution of pure Mg decreased with increasing pH. However, both of these studies relied on the hydrogen evolution method to measure corrosion rates, and recent studies have indicated that this method may not be as reliable as we would like in simulated body fluids [59]. Consequently, it is advisable to measure the corrosion of Mg alloys by multiple methods simultaneously [5].

1.3 Influence of flow

The influence of flow on the biocorrosion of Mg alloys has also been considered previously by Hiromoto et al. [35], Wang et al. [39], Zhen et al. [60], and shown to increase the corrosion rate. However, these studies used free systems, without the influence of an apparatus for hydrogen collection. The use of hydrogen evolution to determine the corrosion rate of Mg alloys has been effective in NaCl solutions [61, 62] and can provide useful insights in synthetic body fluids regarding the time dependence of the corrosion rate, despite the known limitations of this technique in synthetic body fluids [59, 61]. This technique requires an apparatus above the Mg sample to capture the evolved hydrogen. This apparatus changes the fluid flow around the sample, and this influence has not been studied.

1.4 Recent relevant research

Understanding of the *in vivo* corrosion of Mg alloys should be enhanced by an expanded base knowledge in the field of magnesium corrosion. The following are relevant reviews [5, 59, 61, 63-65], and recent works [4, 47, 50, 66-76].

1.5 Research aims

The objectives of this study were:

1. To determine the influence of pH of a simulated body fluid on the corrosion rate of the three magnesium alloys: high-purity magnesium (HP Mg), AZ91 and ZE41.
2. To determine the influence of flow on the corrosion behaviour, by a comparison of specimens in a semi-stagnant condition and specimens freely suspended in a mild-flow condition.

ACCEPTED MANUSCRIPT

2.0 Materials and Methods

2.1 Experimental apparatus

Fig. 1 displays a schematic of the experimental apparatus used for the immersion tests. Four specimens of each alloy (HP Mg, AZ91 and ZE41) were used for each immersion experiment. Table 1 presents the chemical composition by weight% of each alloy. The HP Mg and ZE41 samples were 20 mm long, with a rectangular cross section of 7-8 mm by 7-8 mm. The AZ91 samples were slightly shorter, being approximately 18 mm long with a larger cross section of 8-9 mm by 10-12 mm. Each specimen surface was ground to 1200 grit. The specimens were stored in a desiccator prior to the immersion tests to ensure a uniform surface condition.

The tanks were filled with 10 L of Hanks' solution, made from Sigma-Aldrich Hanks' solution salt, distilled water and sodium hydroxide (reagent grade). Table 2 provides the composition of Hanks' solution in terms of the chemical compounds used to make up the solution [3]. Several hours prior to commencing each immersion tests, the tank was placed in a water bath set at 40.5 °C in order to increase the temperature of the testing solution to 37 ± 1 °C. Sufficient sodium hydroxide or carbon dioxide was added to the testing solution prior to commencing the immersion test to ensure the appropriate pH for that immersion test. The solution was pumped from tank 1 into tank 2, from which the overflow flowed back to tank 1. This fluid flow was created in order to maintain the homogeneity of the chemical composition of the synthetic body fluid (SBF).

The Hanks' solution was buffered to the specified pH of the test with carbon dioxide, utilising the same bicarbonate buffer system as in the human body [77]. The pH was controlled using a pH controller to provide a controlled delivery of CO_2. The solution pH was measured using a glass electrode pH probe in tank 1. This provided the input signal to the pH controller, which caused CO_2 delivery when the pH increased above the set pH value. The released CO_2 dissolved in the solution, forming carbonic acid, which dissociated to bicarbonate and H^+ ions, as summarised by Eq. (2), and thereby the pH was decreased. The amount of pH decrease was related to the amount of CO_2 provided to the solution.

$$H_2O + CO_2 \leftrightarrow H_2CO_3 \leftrightarrow H^+ + HCO_3^- \quad (2)$$

ACCEPTED MANUSCRIPT

2.2 Immersion test methodology

Two specimens of each alloy were suspended in tank 1 using fishing line. These specimens were designated as 1 and 2 (i.e. HP Mg-1, HP Mg-2 etc). Similarly, two specimens of each alloy were suspended by fishing line beneath the up-turned filter funnels in tank 2, approximately 5 mm from the tank base, to enable fluid circulation. These were designated as 3 and 4 (i.e. HP Mg-3, HP Mg-4, etc).

The specimens, and solution, were monitored at least daily. The hydrogen evolution volume was measured visually to a precision of 0.05 mL. The temperature and pH of the solution were monitored, recorded, and adjusted as required. The water level in the immersion testing apparatus, and the water bath, were also monitored and corrected daily, to counteract the effects of evaporation. The specimens were immersed for a period of 166 hour.

Corrosion products were removed upon completion of each experiment, by immersion of each specimen in chromic acid (20 %wt CrO3 + 2 %wt AgNO3) until there was no visible reaction. Each specimen was washed with ethanol, dried with hot air, and weighted. The corrosion rate from mass loss, P_m (mm y^{-1}), was evaluated using [2,78,85]:

$$P_m = 2.1\frac{\Delta m}{At} \tag{3}$$

where Δm is the decrease in Mg metal mass (mg), A is the exposed surface area (cm^2), and t is the immersion time in days.

The corrosion rate from evolved hydrogen, P_H (mm y^{-1}), was evaluated using [2,78,85]:

$$P_H = 2.088\frac{V_H}{At} \tag{4}$$

where V_H is the volume of hydrogen evolved in mL, A is the surface area (cm^2), and t is the immersion time measured in days.

The surface morphology of typical corroded specimens was examined using a JEOL 6060LA scanning electron microscope (SEM). The specimens were cleaned with ethanol, blow-dried with hot air and mounted on an aluminium stub with conductive carbon tape. Specimens from the pH 6.9 test were examined as they were deemed to be representative. A single specimen

ACCEPTED MANUSCRIPT

was chosen of each alloy and flow condition. The specimens from tank 1 were: HP Mg-1, AZ91-2, ZE41-1. The specimens from tank 2 were: HP Mg-4, AZ91-3, ZE41-4.

3. Results

3.1 Immersion tests

Fig. 2 presents the measured pH values of the SBF for the immersion period. The pH of the SBF was set at the required pH prior to commencement of each immersion test, with the addition of either carbon dioxide to lower the pH or sodium hydroxide to increase the pH. Despite the use of the CO_2 - bicarbonate buffer system, and the feedback controller based on the measured pH, there was some variation of the pH of the solution during each test.

It had been expected that (i) the solution pH would tend to increase slowly during the corrosion of the Mg alloys because of the low solubility of $Mg(OH)_2$, and (ii) when the pH increased above the set point, as measured by the pH sensor, the controller would trigger a release of carbon dioxide into tank 1, causing a drop in the pH. The magnesium corrosion and the carbon dioxide release would continue in a controlled cycle, so that the pH would be maintained within a narrow band around the desired test pH. Fig. 2 shows that, for the tests with the pH set at 6.5 and 7.0, the pH was indeed maintained in a narrow band close to the desired pH value. In contrast, for the immersion tests with the pH set at 8.0 and 8.5, the solution pH tended to decrease, and the pH was reset to the required value by manual addition of sodium hydroxide, corresponding to the sharp increases in pH value.

Table 3 presents the values of the average pH and average temperature for each immersion test. For the immersion tests with set pH values of 6.5 and 7.0, the average pH values were close to the set value. In contrast, the average pH values for the other two immersion tests were somewhat lower than the set pH values. The average temperatures were slightly lower than the desired temperature of 37 °C, but were within 1 °C of the desired temperature.

3.2 Mass loss

Table 4 presents the mass of each specimen, measured before and after immersion testing, the measured surface area, and the corresponding corrosion rate evaluated from the mass loss, P_m. The data indicated that the corrosion rates of the three magnesium alloys were in the following decreasing order: ZE41 > HP Mg > AZ91. ZE41 experienced corrosion rates an

ACCEPTED MANUSCRIPT

order of magnitude higher than the other magnesium alloys. HP Mg corroded somewhat more quickly than AZ91, however these corrosion rates were comparable.

Figs. 3, 4 and 5 present the data relating to the corrosion behaviour versus pH. These figures present slightly different data as follows. Fig. 3 presents the average values of the corrosion rate (evaluated from mass loss) for all specimens, from both tanks. Fig. 4 presents the corrosion rates (evaluated from mass loss) separately for specimens immersed in tank 1 and in tank 2. Fig. 5 presents the hydrogen evolution data for ZE41.

Fig. 3 presents the data for all specimens. Fig. 3 indicated that the corrosion rate for each alloy decreased with increasing pH. The data were modelled with the stated log-linear regressions.

Fig. 4 presents the average values of the corrosion rates separately for specimens immersed in tank 1 (filled shapes, slow fluid flow) and in tank 2 (open shapes, stagnant flow). The samples immersed in tank 1 (designated as specimens 1 and 2) were suspended freely using fishing line. The specimens in tank 2 (designated as specimens 3 and 4) were suspended beneath the filter funnels, in order to capture the hydrogen evolved during the immersion test. The average corrosion rates measured for ZE41, HP Mg and AZ91 decreased with increasing pH, in agreement with previous studies on HP Mg [57]. The tank 1 specimens (slow fluid flow) had corrosion rates higher than, or within the experimental error of, the tank 2 specimens (stagnant flow conditions).

3.3 Hydrogen evolution

Table 4 also presents the total volume of hydrogen evolved in each test. In a number of cases, the evolved volume of hydrogen was too small to be measured accurately, and in these cases the volume is listed as nm (measurement not meaningful). Table 4 also presents the corresponding corrosion rate, P_H, evaluated using equation (4), and a comparison of the two corrosion rates, P_m and P_H. Whenever there was meaningful data, the corrosion rates, P_H, for the three alloys showed the following trend: ZE41 > HP Mg > AZ91, in agreement with the mass loss data.

Fig. 5 presents the hydrogen evolution data of the ZE41 samples over time for the four pH values. The hydrogen evolution rate for ZE41 increased initially slowly during the first 50 hours of immersion, after which the evolution rate increased substantially. This can be

ACCEPTED MANUSCRIPT

attributed to an incubation period in which the initial surface films were partially protective and break down, leading to the steady state corrosion indicated by the later linear trend.

The hydrogen evolution data for HP Mg and AZ91 is not presented in a similar fashion, as no useful information was gained due to the low levels of hydrogen evolved from these alloys.

Table 4 allows a comparison for ZE41, between the corrosion rate measured from mass loss, P_m, and the corrosion rate measured from the evolved hydrogen, P_H, over the four tested pH values. The ratio P_H / P_m was consistently in the range 0.4 to 0.6, and the average ratio was ~ 0.5.

3.4 Corrosion Morphology

Figs. 6(a) to (f) present SEM images of typical corroded surfaces for each alloy. Figs. 6(a) to (c) present the surfaces for specimens freely suspected in tank 1 (slow fluid flow). Figs. 6(d) to (f) present the surfaces for the specimens suspended beneath the hydrogen capture funnels in tank 2 (stagnant flow conditions), in which case the solution flow was somewhat less than in tank 1. The corrosion morphology was more locally intense for the specimens immersed in tank 2 (Figs 6d-f) even though the mass loss data indicated that the corrosion rates in tank 2 were lower than those in tank 1, (see Fig. 4).

Figs. 6(a) and 6(d) present the SEM images of the corroded HP Mg specimens. The corrosion was predominantly uniform for both specimens. The specimen immersed in tank 1 had relatively uniform corrosion, with some filiform corrosion. In contrast, the corrosion was deeper for the specimen immersed in tank 2, with some localised corrosion.

Figs. 6(b) and 6(e) present the SEM images of the corroded AZ91 specimens. The corrosion was less uniform than for the HP Mg specimens, with more localised corrosion. There was significantly more localised corrosion on the specimen immersed in tank 2. The degradation on the surface of the AZ91 specimens appeared to be less than that experienced by either HP Mg or ZE41.

Figs. 6(c) and 6(f) present the SEM images of the corroded ZE41 specimens. The corrosion was more significant than for the other two alloys. The corrosion for the specimen immersed in tank 1 was more uniform than that on the specimen immersed in tank 2, which had patches of significant corrosion. Both specimens showed evidence of corrosion associated with a second phase.

ACCEPTED MANUSCRIPT

4. Discussion

4.1 Solution pH values

As the magnesium specimens corrode, Eq. (1) indicates that magnesium hydroxide ($Mg(OH)_2$) is produced. The low solubility of $Mg(OH)_2$ causes the pH to tend to increase to 10.3 [63] The increased pH also tends to stabilise the surface films on the surface of Mg alloys [79, 80].

However, it was desired that the pH be maintained at a constant value in the experiments carried out in this research. To counteract the increase in pH due to Mg corrosion, a controlled amount of CO_2 was allowed to flow into the solution, to decrease the pH as presented in Eq. (2).

The chemistry of the pH of the CO_2 – bicarbonate buffer of Hanks' solution was explored by Zainal Abidin et al. [2]. This analysis indicated that the buffer delivers a pH value of 7.4 for a CO_2 partial pressure of 0.013 atm, and it was experimentally shown that the pH was maintained at a constant value during Mg corrosion. The chemistry of the solution pH indicates that lower pH values result at higher partial pressures of CO_2.

In the present experiments, the pH control was good for pH set values of 6.5 and 7.0, but was poor for pH set values of 7.5 and 8.5. Particularly for the experiments with a set pH value of 8.5, it was observed that the pH value had drifted to lower values overnight. This was attributed to the slow reaction of CO_2 and inadequate mixing. The pH was adjusted by the addition of NaOH. Better pH control would be expected if the Mg corrosion rate had been higher, or with increased stirring of the solution during addition of CO_2.

Eq. (2) indicates that the dissolution of CO_2 releases hydrogen ions into the solution, lowering the pH. Bicarbonate can dissociate further into carbonate and another hydrogen ion. However, this reaction is unlikely to occur in the pH range of the current experiments. The dominant species in the dissociation of carbonic acid is dependent on the pH of the solution. The dominant species in the physiological pH range is bicarbonate [77].

Fig. 2 indicates that the pH deviated from the set value for the experiments with set pH values of 7.5 and 8.5. The CO_2 released into tank 1 to lower the pH was quite slow to react with the solution to achieve a uniform concentration throughout both tanks, as the solution was being stirred at a low flow rate. This resulted in a larger than required amount of CO_2 being

ACCEPTED MANUSCRIPT

released. Due to the slow reaction rate and inhomogeneous CO_2 distribution, by the time the pH sensor had registered the required drop in pH, more than the required volume of CO_2 had been released. This caused the pH to continue to fall after the CO_2 had stopped flowing, as is clear from the decreases in pH over time depicted in Fig. 2.

The pH control was better during the lower pH tests as the solution was more effectively buffered at these lower pH values. The bicarbonate and CO_2 in the solution formed a buffer system known as the bicarbonate buffer system. This is the same buffer system present in the human respiratory system. The pH of a buffer solution can be determined using the Henderson-Hasselbalch equation [81].

$$\mathrm{pH} = -\log(\mathrm{Ka}) + \log\left(\frac{[\mathrm{A}^-]}{[\mathrm{HA}]}\right) = \mathrm{pKa} + \log\left(\frac{[\mathrm{A}^-]}{[\mathrm{HA}]}\right) \tag{5}$$

The acid dissociation constant, K_a, is a measure of how much an acid dissociates when dissolved in a solution. The concentration of the acid is measured as [HA], and the concentration of the conjugate base is $[A^-]$. The *pK*a is of particular significance, as this represents the pH value at which the system is most effectively buffered.

The Henderson-Hasselbalch equation for the dissociation of carbonic acid is:

$$\mathrm{pH} = \mathrm{pKa}_{\mathrm{H_2CO_3}} + \log\left(\frac{[\mathrm{HCO_3^-}]}{[\mathrm{H_2CO_3}]}\right) \tag{6}$$

The *pK*a value for carbonic acid is temperature dependant, and is 6.30 at 37 °C [82]. This is substituted into Eq. (6) to give the Henderson-Hasselbalch equation for the bicarbonate buffer system:

$$\mathrm{pH} = 6.30 + \log\left(\frac{[\mathrm{HCO_3^-}]}{[\mathrm{H_2CO_3}]}\right) \tag{7}$$

This is the buffering equation of the bicarbonate buffer system at 37 °C. The *pK*a value for carbonic acid at 37 °C is 6.30, which is mildly acidic. This means that the buffer is most effective around this value. This is believed to have contributed to the deviations in pH for the higher pH tests.

ACCEPTED MANUSCRIPT

The pH 6.5 and 7.0 tests were within the effective range of the buffer system, and this kept the pH relatively stable. The pH 7.5 and 8.5 tests were outside the effective range of the buffer, and as such were more prone to the shifts in pH caused by the excessive addition of CO_2. Despite the deviations in pH in the latter two tests, the data are nevertheless useful, as the average pH values spanned a good range.

4.2 Influence of pH on the corrosion rate

Fig. 3 shows that the average corrosion rate for HP Mg, AZ91 and ZE41 decreased with increasing solution pH. As Mg corrodes in an unbuffered chloride solution, the pH increases within a few hours to ~10.3 [63] because of the low solubility of $Mg(OH)_2$. There is a partially protective surface film, consisting of a thin layer of MgO at the Mg surface (~1 nm in thickness) with a fairly voluminous second film layer of $Mg(OH)_2$. In the buffered Hanks' solution, the film composition is somewhat different, and is less protective. The active buffer is CO_2 interacting with the bicarbonate ions. In both cases, the corrosion occurs preferentially at breaks in the surface film. The decrease in Mg corrosion rate with increasing pH is attributed to the film becoming more protective as the solution pH increases. The film formed on the surface of AZ91 has been shown to be several times thicker in a solution of pH 12.0 than in air, and the thickness of the film increased with pH [83]. A similar phenomenon is expected to occur for HP Mg and ZE41. A more stable surface layer on the surface would be expected to better protect the surface from corrosion, thereby decreasing corrosion rate.

The increased stability of the surface layer is partly due to the common ion effect. The solubility of the magnesium corrosion product magnesium hydroxide is influenced by the concentration of magnesium and hydroxide ions in the solution. The higher concentrations of hydroxide ions at higher pH values means that magnesium hydroxide precipitates at a lower Mg^{2+} concentration, allowing creation of a more stable layer on the surface.

4.3 Influence of solution flow on the corrosion rate

Fig. 4 indicates that the specimens suspended freely in tank 1 and exposed to a slowly flowing solution had corrosion rates, P_m, somewhat higher than (or equal to) those of the specimens exposed to stagnant solutions suspended beneath the hydrogen capture funnels in tank 2. This difference in corrosion rates was small, but was statistically significant, though was not present in all tests. The difference is attributed to the differences in flow conditions: slowly flowing solution compared with stagnant conditions. This attribution is supported by

ACCEPTED MANUSCRIPT

the work of Hiromoto et al. [35] who found that fluid flow prevented corrosion products from accumulating on specimen surfaces. Reducing the amount of surface corrosion product is expected to increase the corrosion rate.

Wang et al. [39] conducted a study varying flow conditions across Mg alloy plates and stents, in order to determine the influence of flow induced shear stress (FISS) on the corrosion rate of the samples. Increased flow created increased the FISS, and increased the corrosion rate [39], which is consistent with the current study. However, in contrast to the current study, Wang et al. [39] found increasing tendency for pitting and erosion corrosion for the faster flow. This difference is attributed to the small difference between the flow conditions in the current study. The flow rate of the pump was set to be low, and the differences in corrosion rates were small. It is believed that the removal of the corrosion product was the dominant influence on the corrosion rate, as the small difference in FISS between the samples would have likely been much smaller than that measured in the study of Wang et al. [39]. While the mechanics underpinning the influence of flow on corrosion of Mg alloys are still being understood, these studies do identify that flow increases the corrosion rate for Mg alloys. This is consistent with the know influences of flow increasing corrosion in other corroding systems [84].

4.4 Comparison of the corrosion rates P_H and P_m

The presentation of the data in section 3.3 indicated that Table 4 allows a comparison to be made for ZE41 between the corrosion rates measured by mass loss, P_m, and from the evolved hydrogen, P_H. P_H was less than P_m, and the ratio P_H / P_m was in the range 0.4 to 0.6. This ratio is consistent with literature, in that P_H (in SBF with physiological pH and temperature values), was linearly related to P_m, but was consistently lower [2-4, 37, 50]. This is in comparison with NaCl solutions saturated with $Mg(OH)_2$ where there is good agreement between P_H and P_m, except at low corrosion rates [37, 59]. Fig. 7 presents this relationship between P_H and P_m for Mg alloys immersed in SBF at physiological pH and temperature, over a range of studies. This figure is adapted from the figure presented by Taltavull et al. [50], where the data from Taltavull et al. [50] (stars), Kirkland et al. [37] (triangles), and Zainal Abidin et al. [2, 4] (circles, squares) were collated and compared. The ZE41 data from this study (diamonds) was added. The average ratio of ~ 0.5 was plotted as a solid trend line, the theoretical 1:1 ratio was plotted as a dashed line. Fig. 7 indicates that the data of the

ACCEPTED MANUSCRIPT

current study were in good agreement with previous studies when a comparison between P_H and P_m was possible.

The difference between P_H and P_m in SBF with physiological pH values, is attributed to the dissolution of some hydrogen in the Mg sample, and that this dissolution is easier in the SBF because of a less protective surface film that also provides less impedance to hydrogen entry into the Mg specimen [2,50,86].

4.5 Corrosion Morphology

The samples in tank 1 (freely suspended with slow fluid flow) were more uniformly corroded than those in tank 2 (suspended in stagnant flow conditions under the hydrogen burette) for all three alloys. These results indicate that fluid flow influenced the corrosion rate and surface morphology. A lack of fluid flow across the metal surface can lead to a build-up of corrosion product, which decreased the corrosion rate. This build-up of corrosion product may be uneven, and may cause corrosion to form locally, via a crevice corrosion mechanism, and prevent uniform surface attack [35]. Indeed Shi and Atrens [85] identified crevice corrosion for HP Mg.

Although the influence of fluid flow was small on the corrosion rate and corrosion morphology, nevertheless, it is an important effect because medical applications involve the implant in the proximity of blood flow. For this reason, dynamic immersion tests are suggested [39,60].

4.6 Influence of Mg alloy composition and microstructure

Figs. 3 and 4 and indicate that the average corrosion rates of the three magnesium alloys were in the following decreasing order: ZE41 > HP Mg > AZ91. ZE41 experienced average corrosion rates an order of magnitude higher than the other magnesium alloys. HP Mg and AZ91 had more comparable average corrosion rates, but HP Mg corroded consistently more quickly.

There are two main factors that control the corrosion of Mg alloys: (i) surface films and (2) second phases. In chloride solutions [59, 61] the corrosion rate of Mg alloys is greater than that of high-purity Mg because of the micro-galvanic acceleration of the corrosion rate by the second phases. Liu et al. [87] showed that in Mg-Y alloys, the corrosion rate in a chloride solution increased with Y content because of the increasing amount of second phase in the

ACCEPTED MANUSCRIPT

microstructure. In contrast, in a sulphate solution, at high Y contents the corrosion rate decreased with increasing Y content, attributed to a more protective surface film.

The much faster corrosion rates of ZE41 are attributed to the two-phase microstructure and to the relatively poorly protective surface films.

The fact that AZ91 had corrosion rates consistently lower than those of HP Mg is attributed to more protective surface films on the surface of AZ91 (due to the Al content). Moreover, the influence of these films was more important than the influence of the two-phase microstructure of the AZ91.

5. Conclusions

1. The corrosion rates of HP Mg, AZ91 and ZE41 decreased with increasing pH.
2. The corrosion rates of the three magnesium alloys were in the following decreasing order: ZE41 > HP Mg > AZ91. ZE41 experienced corrosion rates an order of magnitude higher than the other magnesium alloys. HP Mg and AZ91 had more comparable corrosion rates, but HP Mg corroded consistently more quickly.
3. A slow fluid flow caused a slightly higher corrosion rate, and a more uniform corrosion morphology for all the Mg alloys.
4. For ZE41 the ratio P_H / P_m was ~ 0.5, where P_H is the corrosion rate measured from the evolved hydrogen, and P_m is the corrosion rate measured from mass loss.

ACCEPTED MANUSCRIPT

6. References

[1] F. Witte, J. <PN>Fischer</PN>, J. Nellesen, H.-A. Crostack, V. Kaese, A. Pisch, F. Beckmann, H. Windhagen, In vitro and in vivo corrosion measurements of magnesium alloys, Biomaterials, 27 (2006) 1013-1018.

[2] N.I.Z. Abidin, A.D. Atrens, D. Martin, A. Atrens, Corrosion of high purity Mg, Mg2Zn0. 2Mn, ZE41 and AZ91 in Hank's solution at 37 C, Corrosion Science, 53 (2011) 3542-3556.

[3] N.I.Z. Abidin, D. Martin, A. Atrens, Corrosion of high purity Mg, AZ91, ZE41 and Mg2Zn0. 2Mn in Hank's solution at room temperature, Corrosion Science, 53 (2011) 862-872.

[4] N.I.Z. Abidin, B. Rolfe, H. Owen, J. Malisano, D. Martin, J. Hofstetter, P.J. Uggowitzer, A. Atrens, The in vivo and in vitro corrosion of high-purity magnesium and magnesium alloys WZ21 and AZ91, Corrosion Science, 75 (2013) 354-366.

[5] A. Atrens, M. Liu, N.I.Z. Abidin, Corrosion mechanism applicable to biodegradable magnesium implants, Materials Science and Engineering: B, 176 (2011) 1609-1636.

[6] M.P. Staiger, A.M. Pietak, J. Huadmai, G. Dias, Magnesium and its alloys as orthopedic biomaterials: a review, Biomaterials, 27 (2006) 1728-1734.

[7] M. Ascencio, M. Pekguleryuz, S. Omanovic, An investigation of the corrosion mechanisms of WE43 Mg alloy in a modified simulated body fluid solution: The effect of electrolyte renewal, Corrosion Science, 91 (2015) 297-310.

ACCEPTED MANUSCRIPT

[8] M. Ascencio, M. Pekguleryuz, S. Omanovic, An investigation of the corrosion mechanisms of WE43 Mg alloy in a modified simulated body fluid solution: The influence of immersion time, Corrosion Science, 87 (2014) 489-503.

[9] M. Carboneras, M.C. García-Alonso, M.L. Escudero, Biodegradation kinetics of modified magnesium-based materials in cell culture medium, Corrosion Science, 53 (2011) 1433-1439.

[10] T.F. da Conceição, N. Scharnagl, W. Dietzel, K.U. Kainer, Controlled degradation of a magnesium alloy in simulated body fluid using hydrofluoric acid treatment followed by polyacrylonitrile coating, Corrosion Science, 62 (2012) 83-89.

[11] F. El-Taib Heakal, O.S. Shehata, N.S. Tantawy, Degradation behaviour of AZ80E magnesium alloy exposed to phosphate buffer saline medium, Corrosion Science, 86 (2014) 285-294.

[12] G. Han, J.-Y. Lee, Y.-C. Kim, J.H. Park, D.-I. Kim, H.-S. Han, S.-J. Yang, H.-K. Seok, Preferred crystallographic pitting corrosion of pure magnesium in Hanks' solution, Corrosion Science, 63 (2012) 316-322.

[13] J. Hofstetter, E. Martinelli, A.M. Weinberg, M. Becker, B. Mingler, P.J. Uggowitzer, J.F. Löffler, Assessing the degradation performance of ultrahigh-purity magnesium in vitro and in vivo, Corrosion Science, 91 (2015) 29-36.

[14] M. Jamesh, G. Wu, Y. Zhao, P.K. Chu, Effects of silicon plasma ion implantation on electrochemical corrosion behavior of biodegradable Mg–Y–RE Alloy, Corrosion Science, 69 (2013) 158-163.

ACCEPTED MANUSCRIPT

[15] M.I. Jamesh, G. Wu, Y. Zhao, D.R. McKenzie, M.M.M. Bilek, P.K. Chu, Electrochemical corrosion behavior of biodegradable Mg–Y–RE and Mg–Zn–Zr alloys in Ringer's solution and simulated body fluid, Corrosion Science, 91 (2015) 160-184.

[16] M.I. Jamesh, G. Wu, Y. Zhao, D.R. McKenzie, M.M.M. Bilek, P.K. Chu, Effects of zirconium and oxygen plasma ion implantation on the corrosion behavior of ZK60 Mg alloy in simulated body fluids, Corrosion Science, 82 (2014) 7-26.

[17] H. Kalb, A. Rzany, B. Hensel, Impact of microgalvanic corrosion on the degradation morphology of WE43 and pure magnesium under exposure to simulated body fluid, Corrosion Science, 57 (2012) 122-130.

[18] H.S. Kim, G.H. Kim, H. Kim, W.J. Kim, Enhanced corrosion resistance of high strength Mg–3Al–1Zn alloy sheets with ultrafine grains in a phosphate-buffered saline solution, Corrosion Science, 74 (2013) 139-148.

[19] T. Lei, W. Tang, S.-H. Cai, F.-F. Feng, N.-F. Li, On the corrosion behaviour of newly developed biodegradable Mg-based metal matrix composites produced by in situ reaction, Corrosion Science, 54 (2012) 270-277.

[20] G. Liu, S. Tang, D. Li, J. Hu, Self-adjustment of calcium phosphate coating on micro-arc oxidized magnesium and its influence on the corrosion behaviour in simulated body fluids, Corrosion Science, 79 (2014) 206-214.

[21] N. Ott, P. Schmutz, C. Ludwig, A. Ulrich, Local, element-specific and time-resolved dissolution processes on a Mg–Y–RE alloy – Influence of inorganic species and buffering systems, Corrosion Science, 75 (2013) 201-211.

ACCEPTED MANUSCRIPT

[22] P. Pérez, E. Onofre, S. Cabeza, I. Llorente, J.A. del Valle, M.C. García-Alonso, P. Adeva, M.L. Escudero, Corrosion behaviour of Mg–Zn–Y–Mischmetal alloys in phosphate buffer saline solution, Corrosion Science, 69 (2013) 226-235.

[23] S. Shanmugam, T.S.N. Sankara Narayanan, P. Mohan Sathyaraj, K. Ravichandran, M.H. Lee, Spectrophotometric analysis to monitor the corrosion behaviour of magnesium during immersion corrosion testing: A suitable alternative to pH measurement?, Corrosion Science, 89 (2014) 338-342.

[24] Y. Xin, T. Hu, P.K. Chu, Degradation behaviour of pure magnesium in simulated body fluids with different concentrations of, Corrosion Science, 53 (2011) 1522-1528.

[25] D. Zander, N.A. Zumdick, Influence of Ca and Zn on the microstructure and corrosion of biodegradable Mg–Ca–Zn alloys, Corrosion Science, 93 (2015) 222-233.

[26] R.-C. Zeng, Y. Hu, S.-K. Guan, H.-Z. Cui, E.-H. Han, Corrosion of magnesium alloy AZ31: The influence of bicarbonate, sulphate, hydrogen phosphate and dihydrogen phosphate ions in saline solution, Corrosion Science, 86 (2014) 171-182.

[27] N.T. Kirkland, J. Lespagnol, N. Birbilis, M.P. Staiger, A survey of bio-corrosion rates of magnesium alloys, Corrosion Science, 52 (2010) 287-291.

[28] R.-C. Zeng, L. Sun, Y.-F. Zheng, H.-Z. Cui, E.-H. Han, Corrosion and characterisation of dual phase Mg–Li–Ca alloy in Hank's solution: The influence of microstructural features, Corrosion Science, 79 (2014) 69-82.

[29] M. Bornapour, N. Muja, D. Shum-Tim, M. Cerruti, M. Pekguleryuz, Biocompatibility and biodegradability of Mg–Sr alloys: The formation of Sr-substituted hydroxyapatite, Acta Biomaterialia, 9 (2013) 5319-5330.

ACCEPTED MANUSCRIPT

[30] Y. Chen, Z. Xu, C. Smith, J. Sankar, Recent advances on the development of magnesium alloys for biodegradable implants, Acta Biomaterialia, 10 (2014) 4561-4573.

[31] L. Choudhary, R.K. Singh Raman, Magnesium alloys as body implants: Fracture mechanism under dynamic and static loadings in a physiological environment, Acta Biomaterialia, 8 (2012) 916-923.

[32] D. Dziuba, A. Meyer-Lindenberg, J.M. Seitz, H. Waizy, N. Angrisani, J. Reifenrath, Long-term in vivo degradation behaviour and biocompatibility of the magnesium alloy ZEK100 for use as a biodegradable bone implant, Acta Biomaterialia, 9 (2013) 8548-8560.

[33] S.F. Fischerauer, T. Kraus, X. Wu, S. Tangl, E. Sorantin, A.C. Hänzi, J.F. Löffler, P.J. Uggowitzer, A.M. Weinberg, In vivo degradation performance of micro-arc-oxidized magnesium implants: A micro-CT study in rats, Acta Biomaterialia, 9 (2013) 5411-5420.

[34] S. Hiromoto, M. Inoue, T. Taguchi, M. Yamane, N. Ohtsu, In vitro and in vivo biocompatibility and corrosion behaviour of a bioabsorbable magnesium alloy coated with octacalcium phosphate and hydroxyapatite, Acta Biomaterialia, 11 (2015) 520-530.

[35] S. Hiromoto, A. Yamamoto, N. Maruyama, H. Somekawa, T. Mukai, Influence of pH and flow on the polarisation behaviour of pure magnesium in borate buffer solutions, Corrosion Science, 50 (2008) 3561-3568.

[36] Y. Jang, B. Collins, J. Sankar, Y. Yun, Effect of biologically relevant ions on the corrosion products formed on alloy AZ31B: An improved understanding of magnesium corrosion, Acta Biomaterialia, 9 (2013) 8761-8770.

ACCEPTED MANUSCRIPT

[37] N.T. Kirkland, N. Birbilis, M.P. Staiger, Assessing the corrosion of biodegradable magnesium implants: A critical review of current methodologies and their limitations, Acta Biomaterialia, 8 (2012) 925-936.

[38] X. Lin, L. Tan, Q. Zhang, K. Yang, Z. Hu, J. Qiu, Y. Cai, The in vitro degradation process and biocompatibility of a ZK60 magnesium alloy with a forsterite-containing micro-arc oxidation coating, Acta Biomaterialia, 9 (2013) 8631-8642.

[39] J. Wang, V. Giridharan, V. Shanov, Z. Xu, B. Collins, L. White, Y. Jang, J. Sankar, N. Huang, Y. Yun, Flow-induced corrosion behavior of absorbable magnesium-based stents, Acta Biomaterialia, 10 (2014) 5213-5223.

[40] Y. Xin, T. Hu, P.K. Chu, In vitro studies of biomedical magnesium alloys in a simulated physiological environment: A review, Acta Biomaterialia, 7 (2011) 1452-1459.

[41] Y. Zhao, M.I. Jamesh, W.K. Li, G. Wu, C. Wang, Y. Zheng, K.W.K. Yeung, P.K. Chu, Enhanced antimicrobial properties, cytocompatibility, and corrosion resistance of plasma-modified biodegradable magnesium alloys, Acta Biomaterialia, 10 (2014) 544-556.

[42] K. Bobe, E. Willbold, I. Morgenthal, O. Andersen, T. Studnitzky, J. Nellesen, W. Tillmann, C. Vogt, K. Vano, F. Witte, In vitro and in vivo evaluation of biodegradable, open-porous scaffolds made of sintered magnesium W4 short fibres, Acta Biomaterialia, 9 (2013) 8611-8623.

[43] A.H.M. Sanchez, B.J.C. Luthringer, F. Feyerabend, R. Willumeit, Mg and Mg alloys: How comparable are in vitro and in vivo corrosion rates? A review, Acta Biomaterialia, 13 (2015) 16-31.

ACCEPTED MANUSCRIPT

[44] G. Levy, E. Aghion, Effect of diffusion coating of Nd on the corrosion resistance of biodegradable Mg implants in simulated physiological electrolyte, Acta Biomaterialia, 9 (2013) 8624-8630.

[45] F. Witte, The history of biodegradable magnesium implants: a review, Acta Biomaterialia, 6 (2010) 1680-1692.

[46] F. Witte, V. Kaese, H. Haferkamp, E. Switzer, A. Meyer-Lindenberg, C. Wirth, H. Windhagen, In vivo corrosion of four magnesium alloys and the associated bone response, Biomaterials, 26 (2005) 3557-3563.

[47] Z. Abidin, N. Ishida, A. Da Forno, M. Bestetti, D. Martin, A. Beer, A. Atrens, Evaluation of Coatings for Mg Alloys for Biomedical Applications, Advanced Engineering Materials, 17 (2015) 58-67.

[48] M. Staiger, F. Feyerabend, R. Willumeit, C. Sfeir, Y. Zheng, S. Virtanen, W. Müeller, A. Atrens, M. Peuster, P. Kumta, Summary of the panel discussions at the 2nd Symposium on Biodegradable Metals, Maratea, Italy, 2010, Materials Science and Engineering: B, 176 (2011) 1596-1599.

[49] J. Walker, S. Shadanbaz, N.T. Kirkland, E. Stace, T. Woodfield, M.P. Staiger, G.J. Dias, Magnesium alloys: predicting in vivo corrosion with in vitro immersion testing, Journal of Biomedical Materials Research Part B: Applied Biomaterials, 100 (2012) 1134-1141.

[50] C. Taltavull, Z. Shi, B. Torres, J. Rams, A. Atrens, Influence of the chloride ion concentration on the corrosion of high-purity Mg, ZE41 and AZ91 in buffered Hank's solution, Journal of Materials Science: Materials in Medicine, 25 (2014) 329-345.

ACCEPTED MANUSCRIPT

[51] F. Feyerabend, J. <PN>Fischer</PN>, J. Holtz, F. Witte, R. Willumeit, H. Drücker, C. Vogt, N. Hort, Evaluation of short-term effects of rare earth and other elements used in magnesium alloys on primary cells and cell lines, Acta biomaterialia, 6 (2010) 1834-1842.

[52] Y. Ding, C. Wen, P. Hodgson, Y. Li, Effects of alloying elements on the corrosion behavior and biocompatibility of biodegradable magnesium alloys: a review, Journal of Materials Chemistry B, 2 (2014) 1912-1933.

[53] J. Duhm, Effects of 2, 3-diphosphoglycerate and other organic phosphate compounds on oxygen affinity and intracellular pH of human erythrocytes, Pfluegers Archiv, 326 (1971) 341-356.

[54] P. Woodrow, Arterial blood gas analysis, Nursing standard, 18 (2004) 45-52.

[55] K. Alberti, C. Cuthbert, The hydrogen ion in normal metabolism: a review, Metabolic acidosis, (1982) 1-15.

[56] K. Nielsen, Corrosion of metallic implants, British Corrosion Journal, 22 (1987) 272-278.

[57] W. Ng, K. Chiu, F. Cheng, Effect of pH on the in vitro corrosion rate of magnesium degradable implant material, Materials Science and Engineering: C, 30 (2010) 898-903.

[58] Y. Xin, K. Huo, H. Tao, G. Tang, P.K. Chu, Influence of aggressive ions on the degradation behavior of biomedical magnesium alloy in physiological environment, Acta Biomaterialia, 4 (2008).

ACCEPTED MANUSCRIPT

[59] A. Atrens, G.L. Song, M. Liu, Z. Shi, F. Cao, M.S. Dargusch, Review of recent developments in the field of magnesium corrosion, Advanced Engineering Materials, 17 (2015) 400-453.

[60] Z. Zhen, T.-f. Xi, Y.-f. Zheng, A review on in vitro corrosion performance test of biodegradable metallic materials, Transactions of Nonferrous Metals Society of China, 23 (2013) 2283-2293.

[61] G. Song, A. Atrens, Understanding magnesium corrosion—a framework for improved alloy performance, Advanced engineering materials, 5 (2003) 837-858.

[62] G. Song, A. Atrens, D. StJohn, An hydrogen evolution method for the estimation of the corrosion rate of magnesium alloys, Magnesium Technology 2001, (2001) 254-262.

[63] A. Atrens, G.-L. Song, F. Cao, Z. Shi, P.K. Bowen, Advances in Mg corrosion and research suggestions, Journal of Magnesium and Alloys, 1 (2013) 177-200.

[64] N. Winzer, A. Atrens, G. Song, E. Ghali, W. Dietzel, K.U. Kainer, N. Hort, C. Blawert, A critical review of the stress corrosion cracking (SCC) of magnesium alloys, Advanced Engineering Materials, 7 (2005) 659-693.

[65] G.L. Song, A. Atrens, Corrosion mechanisms of magnesium alloys, Advanced engineering materials, (1999) 11-33.

[66] Z. Shi, J. Hofstetter, F. Cao, P.J. Uggowitzer, M.S. Dargusch, A. Atrens, Corrosion and stress corrosion cracking of ultra-high-purity Mg5Zn, Corrosion Science, 93 (2015) 330-335.

ACCEPTED MANUSCRIPT

[67] A.D. Atrens, I. Gentle, A. Atrens, Possible dissolution pathways participating in the Mg corrosion reaction, Corrosion Science, 92 (2014) 173-181.

[68] F. Cao, Z. Shi, G.-L. Song, M. Liu, M.S. Dargusch, A. Atrens, Influence of hot rolling on the corrosion behavior of several Mg–X alloys, Corrosion Science, 90 (2015) 176-191.

[69] C. Taltavull, A. Lopez, B. Torres, A. Atrens, J. Rams, Optimisation of the high velocity oxygen fuel (HVOF) parameters to produce effective corrosion control coatings on AZ91 magnesium alloy, Materials and Corrosion, 66 (2014) 423-433.

[70] Z. Shi, J.X. Jia, A. Atrens, Galvanostatic anodic polarisation of WE43, Journal of Magnesium and Alloys, 2 (2014) 197-202.

[71] Z. Shi, F. Cao, G.-L. Song, A. Atrens, Low apparent valence of Mg during corrosion, Corrosion Science, 88 (2014) 434-443.

[72] C. Taltavull, B. Torres, A. Lopez, P. Rodrigo, E. Otero, A. Atrens, J. Rams, Corrosion behaviour of laser surface melted magnesium alloy AZ91D, Materials & Design, 57 (2014) 40-50.

[73] K. Schlüter, Z. Shi, C. Zamponi, F. Cao, E. Quandt, A. Atrens, Corrosion performance and mechanical properties of sputter-deposited MgY and MgGd alloys, Corrosion Science, 78 (2014) 43-54.

[74] Z. Shi, A. Atrens, Comments on the paper entitled “Observations of the galvanostatic dissolution of pure magnesium” by NT Kirkland, G. Williams and N. Birbilis, Corrosion Science, 77 (2013) 403-406.

ACCEPTED MANUSCRIPT

[75] Z. Shi, F. Cao, G.-L. Song, M. Liu, A. Atrens, Corrosion behaviour in salt spray and in 3.5% NaCl solution saturated with Mg (OH) 2 of as-cast and solution heat-treated binary Mg–RE alloys: RE= Ce, La, Nd, Y, Gd, Corrosion Science, 76 (2013) 98-118.

[76] F. Cao, Z. Shi, G.-L. Song, M. Liu, A. Atrens, Corrosion behaviour in salt spray and in 3.5% NaCl solution saturated with Mg (OH) 2 of as-cast and solution heat-treated binary Mg–X alloys: X= Mn, Sn, Ca, Zn, Al, Zr, Si, Sr, Corrosion Science, 76 (2013) 60-97.

[77] S.J. Choi, J. Lim, Stability of the bicarbonate system in the blood, Journal of Mathematical Analysis and Applications, 356 (2009) 145-153.

[78] Z. Qiao, Z. Shi, N. Hort, N.I.Z. Abidin, A. Atrens, Corrosion behaviour of a nominally high purity Mg ingot produced by permanent mould direct chill casting, Corrosion Science, 61 (2012) 185-207.

[79] G. Song, A. Atrens, D. St John, X. Wu, J. Nairn, The anodic dissolution of magnesium in chloride and sulphate solutions, Corrosion Science, 39 (1997) 1981-2004.

[80] G. Song, A. Atrens, X. Wu, B. Zhang, Corrosion behaviour of AZ21, AZ501 and AZ91 in sodium chloride, Corrosion Science, 40 (1998) 1769-1791.

[81] H.N. Po, N. Senozan, The Henderson-Hasselbalch equation: its history and limitations, Journal of Chemical Education, 78 (2001) 1499.

[82] S. Park, C. Kim, M. Kim, Spectrophotometric measurement of the first dissociation constants of carbonic acid at elevated temperatures, Journal of the <PN>Chemical Society</PN>, Faraday Transactions, 94 (1998) 1421-1425.

ACCEPTED MANUSCRIPT

[83] Y.J. Ko, D.Y. Chang, J.D. Lim, K.S. Shin, Effect of Mg17Al12 precipitate on corrosion behavior of AZ91D magnesium alloy, in: Materials Science Forum, Trans Tech Publ, 2003, pp. 851-856.

[84] D.A. Jones, Principles and prevention of corrosion, Prentice Hall <PL>Upper Saddle River, NJ</PL>, 1996.

[85] Z. Shi, A. Atrens, An innovative specimen configuration for the study of Mg corrosion, Corrosion Science, 53 (2011) 226-246.

[86] K. Nogita, S. Ockert, J. Pierce, M. Greaves, C. Gourlay, A. Dahle, Engineering the Mg–Mg 2 Ni eutectic transformation to produce improved hydrogen storage alloys, international journal of hydrogen energy, 34 (2009) 7686-7691.

[87] M. Liu, P. Schmutz, P.J. Uggowitzer, G. Song, A. Atrens, The influence of yttrium (Y) on the corrosion of Mg–Y binary alloys, Corrosion Science, 52 (2010) 3687-3701.

ACCEPTED MANUSCRIPT

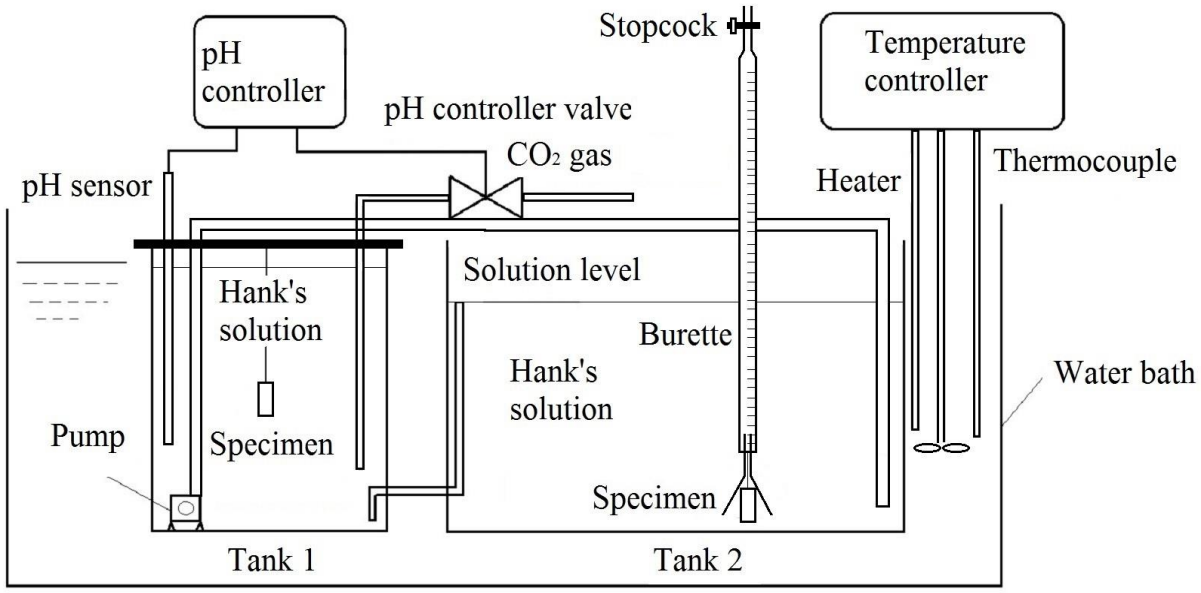

Fig. 1 Schematic of the experiential immersion apparatus.

ACCEPTED MANUSCRIPT

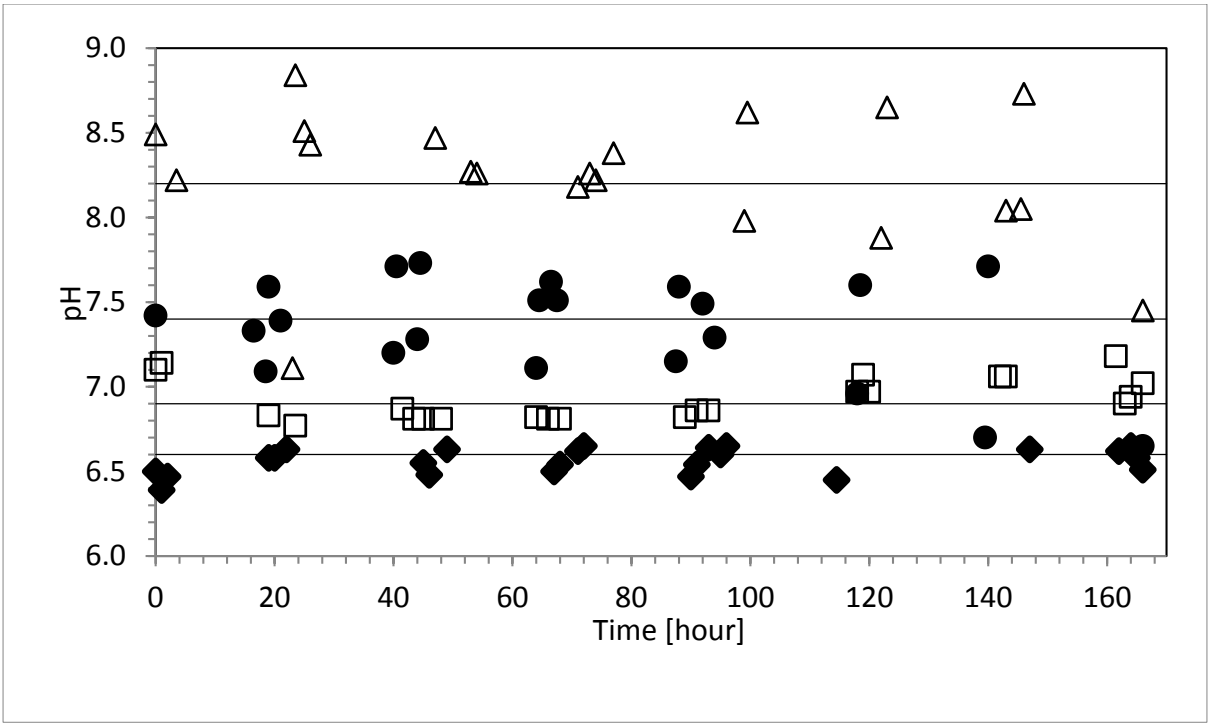

Fig. 2 pH values measured during the four immersion tests, with target pH values of 8.5 (triangles), 7.5 (circles), 7.0 (squares) and 6.5 (diamonds). The measured average pH values were 6.6, 6.9, 7.4 and 8.2, and are presented as the horizontal lines.

ACCEPTED MANUSCRIPT

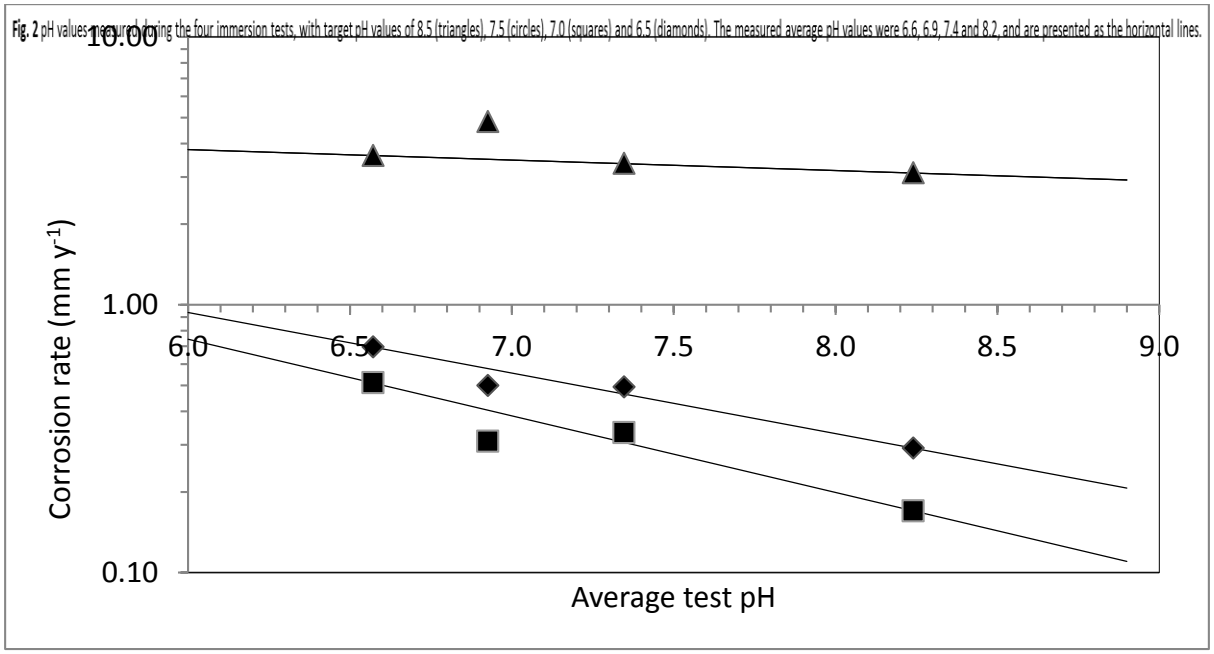

Fig. 3 Average values of the corrosion rate (evaluated from mass loss) for all specimens from both tanks for immersion in CO_2-bicarbonate buffered Hanks' solution at 37 ± 1 °C for 166 h plotted against the average solution pH of the solution. ZE41 (triangles), HP Mg (diamonds) and AZ91 (squares). The trend lines were as follows; [ZE41: $\log(P_m) = -0.039pH + 0.82$, $R^2 = 0.95$], [HP Mg: $\log(P_m) = -0.29pH + 1.6$, $R^2 = 0.85$] and [AZ91: $\log(P_m) = -0.23pH + 1.3$, $R^2 = 0.92$] .

ACCEPTED MANUSCRIPT

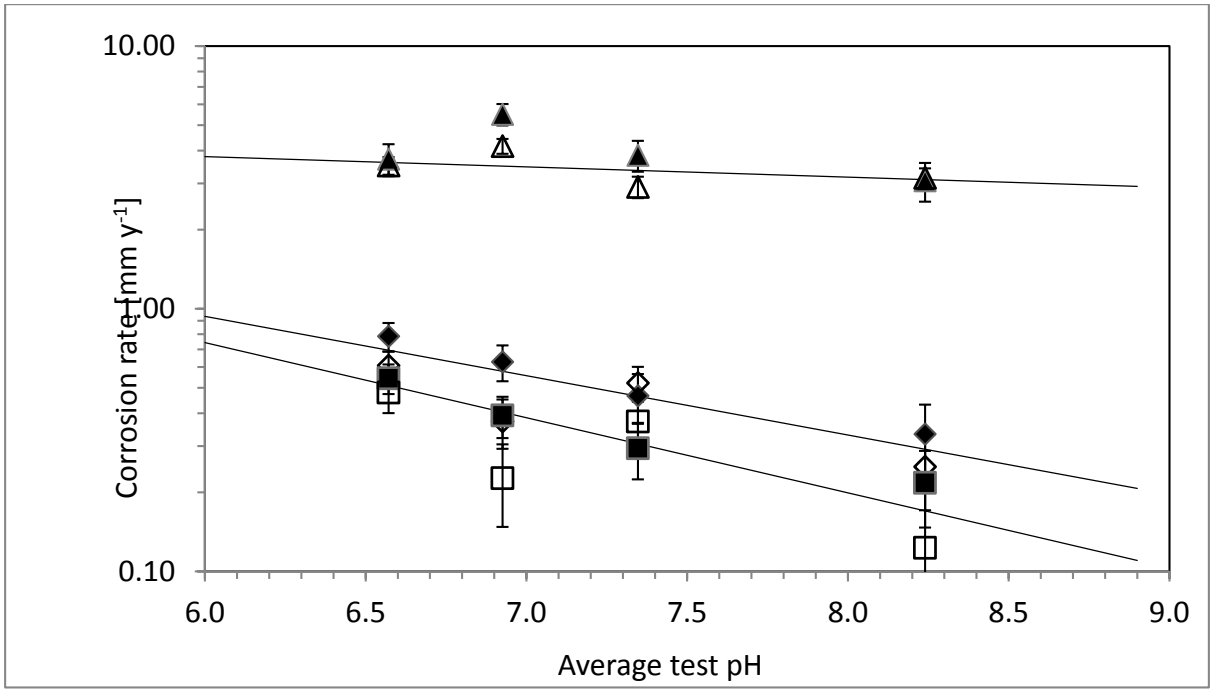

Fig. 4 Average corrosion rate (evaluated from mass loss) for specimens immersed in tank 1 (filled shapes, slow fluid flow) and in tank 2 (open shapes, stagnant flow conditions) for immersion in CO_2-bicarbonate buffered Hanks' solution at a temperature of 37 ± 1°C for 166 h plotted against the average pH of the solution. ZE41 (triangles), HP Mg (diamonds) and AZ91 (squares). Corrosion rates for specimens in tank 1, which were freely suspended (filled shapes), were typically somewhat larger than those of specimens in tank 2 which were suspended beneath hydrogen capture burettes (unfilled shapes). Standard error bars were calculated from the data spread. Trend lines were evaluated in a similar manner to those for Fig. 3 .

ACCEPTED MANUSCRIPT

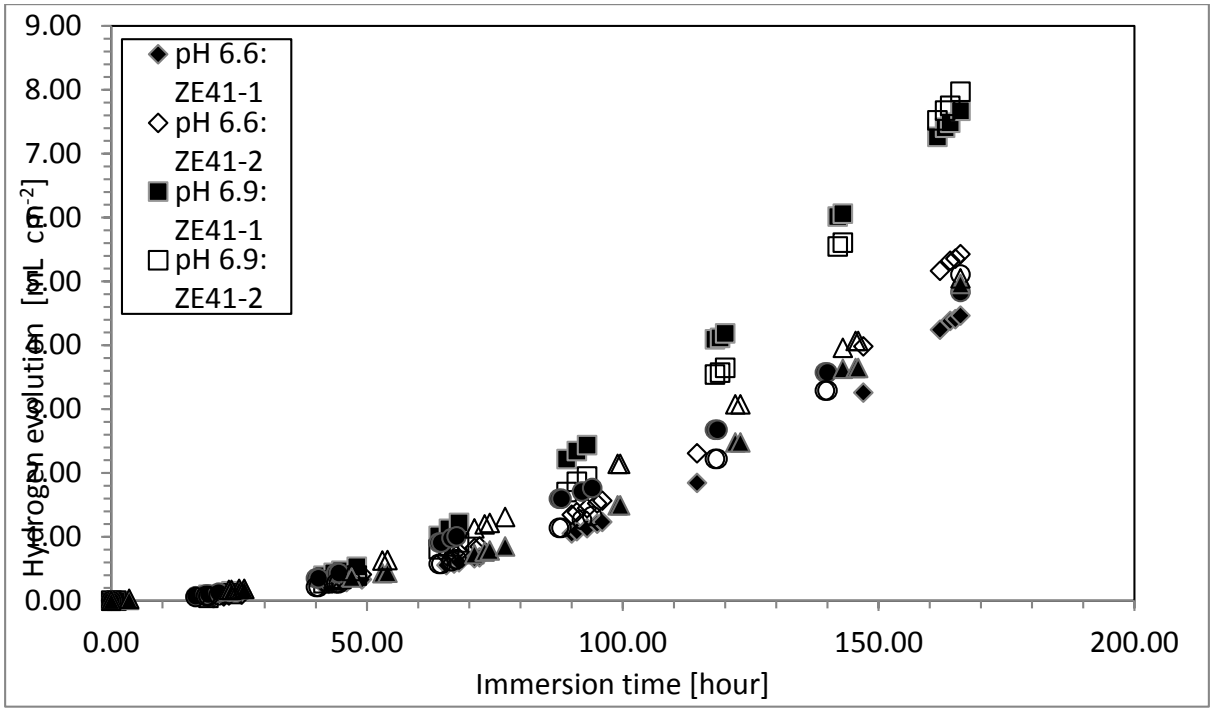

Fig. 5 Hydrogen evolution normalised for surface area for the ZE41 samples immersed in CO_2-bicarbonate buffered Hanks' solution at 37 ± 1 °C for 166 h over four test pH levels: 6.6, 6.9, 7.4 & 8.2.

ACCEPTED MANUSCRIPT

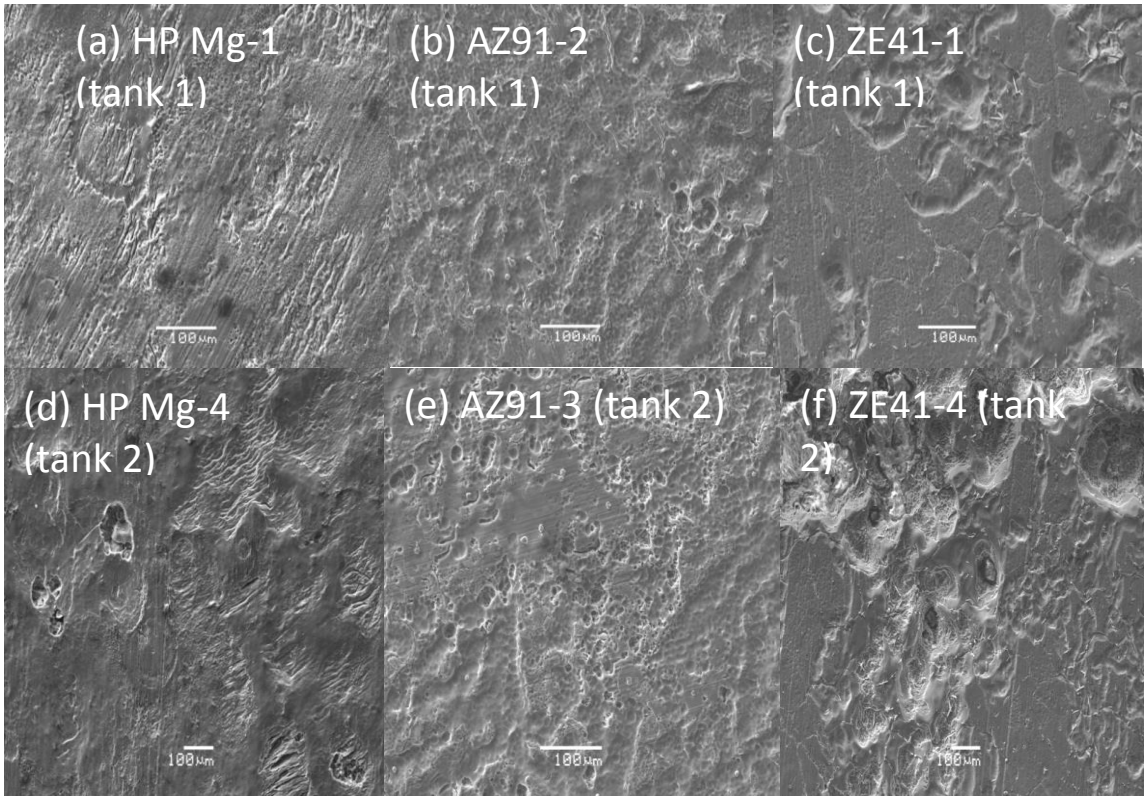

Fig. 6(a-f) Surface appearance of typical specimens of HP Mg, AZ91 and ZE41 after immersion in CO_2-bicarbonate buffered Hanks' solution at 37 ± 1°C and pH 6.9 for 166 h.

ACCEPTED MANUSCRIPT

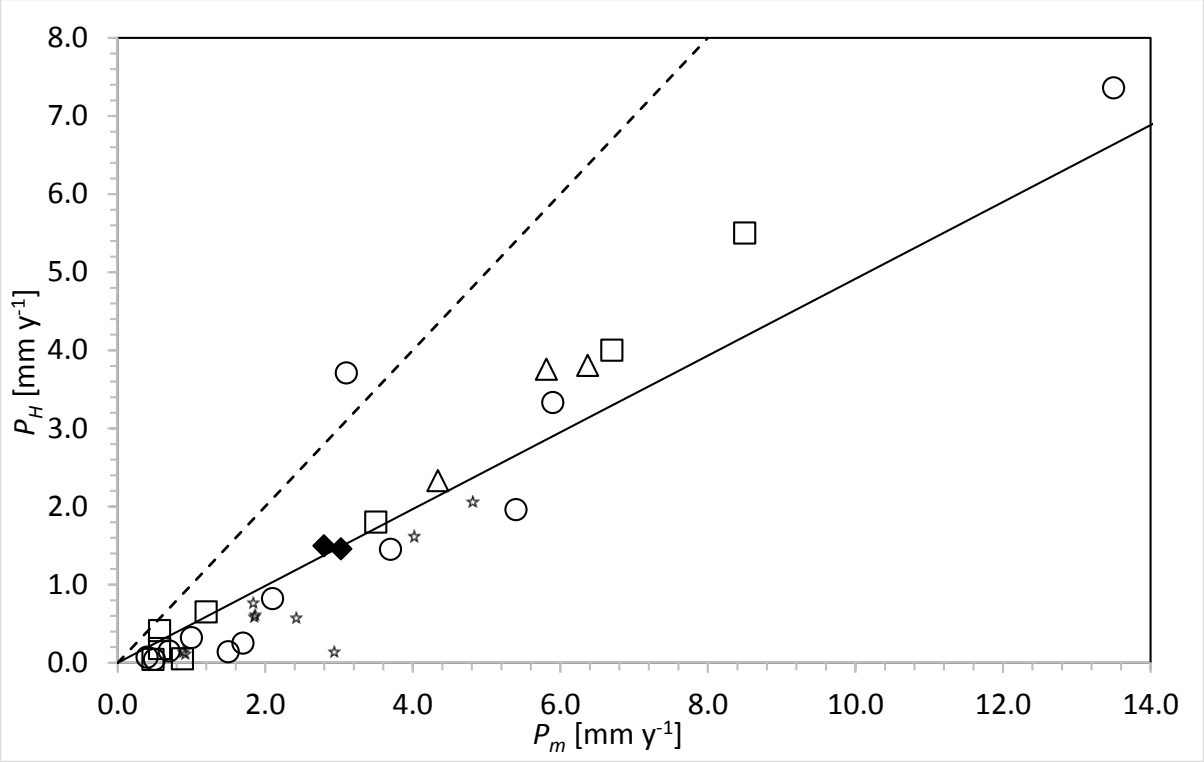

Fig. 7 Comparison between corrosion rates evaluated from the total evolved hydrogen, P_H, and from weight loss, P_m, for alloys immersion tested in Hanks' solution buffered to be close to the physiological pH of 7.4 and at 37°C. Data from current study (diamonds) was added to the original comparison of Taltavull et al. [50]. Other data points were collated from Taltavull et al. [59] (stars), Kirkland et al. [37] (triangles), and Zainal Abidin et al. [2,4] (circles, squares). The solid trend line is the average ratio of P_H / P_m found in this study of ~ 0.5. The dashed trend line represents the theoretical 1/1 ratio calculated from equation (1).

ACCEPTED MANUSCRIPT

Table 1 Chemical composition by % weight of high-purity magnesium (HP Mg), and Mg alloys ZE41 and AZ91

Element	HP Mg	ZE41	AZ91
Mg	Balance	Balance	Balance
Al	0.0088	0.004	8.15
Zn	0.02	4.59	0.64
Ce	<0.01	1.06	<0.01
Mn	0.02	0.02	0.15
Cu	0.002	0.0014	0.001
Fe	0.007	0.0056	0.0046
Ni	0.0001	0.0002	0.0031
Y	<0.01	0.13	<0.01
La	<0.01	0.48	<0.01
Pr	<0.01	0.13	<0.01
Nd	<0.01	0.1	<0.01

ACCEPTED MANUSCRIPT

Ca	<0.01	0.1	<0.01
Be	<0.005	<0.005	<0.01
Sn	-	<0.002	-
Pb	-	<0.002	-
Cr	-	<0.001	-
Zr	-	<0.002	-
Sr	-	<0.001	-
Gd	<0.01	<0.1	<0.01

ACCEPTED MANUSCRIPT

Table 2 Composition in terms of the chemical compounds used to make up Hanks' solution

NaCl	$CaCl_2.2H_2O$	$MgSO_4$ (anhydrous)	KCl	KH_2PO_4 (anhydrous)	Na_2HPO_4 (anhydrous)	D-Glucose	$NaHCO_3$
137	2.5	0.8	5.4	0.4	0.3	5.6	4.2

Table 3 Average pH and average temperature of each test

Designated test pH	Actual average pH	Average temperature (°C)
6.5	6.57	36.2
7	6.93	36.5
7.5	7.35	36.7
8.5	8.24	36.3

ACCEPTED MANUSCRIPT

Table 4 Mass loss data, total evolved hydrogen, associated corrosion rates evaluated from mass loss, P_m, and apparent associated corrosion rates evaluated from the evolved hydrogen, P_H, for magnesium alloys immersed in bicarbonate buffered Hanks' solution for 166 hours, at various actual average pH values. The ratio of (the corrosion rate evaluated from the evolved hydrogen) / (corrosion rates evaluated from mass loss) is given by P_H/ P_m. nm = not meaningful

pH	Specimen designation	m_{before} (g)	m_{after} (g)	Δm (mg)	A_{before} (cm^2)	A_{after} (cm^2)	P_m (mm y^{-1})	Total evolved hydrogen (mL)	P_H (mm y^{-1})	P_H/ P_m
6.6	HP Mg-1	2.2675	2.2436	23.9	7.59	7.53	0.96	-	-	-
	HP Mg-2	2.2539	2.2384	15.5	7.75	7.67	0.61	-	-	-
	HP Mg-3	2.0406	2.0207	19.9	7.56	7.37	0.55	1	0.04	nm
	HP Mg-4	2.2322	2.2154	16.9	7.79	7.7	0.66	2.05	0.08	nm
	AZ91-1	3.517	3.4983	18.7	9.86	9.72	0.58	-	-	-
	AZ91-2	3.6265	3.6098	16.7	10.02	9.98	0.51	-	-	-
	AZ91-3	3.2953	3.2776	17.7	9.36	9.28	0.58	0.75	0.02	nm
	AZ91-4	3.3246	3.3128	11.8	9.44	9.33	0.38	0.45	0.01	nm
	ZE41-1	2.5681	2.4553	112.8	8.69	8.65	3.95	-	-	-

ACCEPTED MANUSCRIPT

	ZE41-2	2.1424	2.0597	82.7	7.23	7.19	3.48	-	-	-
	ZE41-3	2.1328	2.0471	85.7	7.23	7.19	3.61	32.2	1.33	0.37
	ZE41-4	2.1752	2.0934	81.8	7.3	7.25	3.41	39.5	1.62	0.47
	HP Mg-1	1.9305	1.9149	15.6	7.24	7.21	0.66	-	-	-
	HP Mg-2	2.8111	2.7936	17.5	8.94	8.8	0.6	-	-	-
	HP Mg-3	2.6117	2.6006	11.1	8.82	8.65	0.39	nm	-	-
	HP Mg-4	1.9347	1.9259	8.8	7.47	7.42	0.36	nm	-	-
	AZ91-1	2.9663	2.9596	6.7	7.31	7.27	0.28	-	-	-
	AZ91-2	3.3527	3.3397	13	7.8	7.73	0.51	-	-	-
6.9	AZ91-3	3.2893	3.2861	3.2	7.7	7.64	0.13	nm	-	-
	AZ91-4	3.3975	3.3889	8.6	7.9	7.86	0.33	nm	-	-
	ZE41-1	2.5594	2.4113	148.1	7.63	7.52	5.86	-	-	-
	ZE41-2	2.3484	2.2313	117.1	6.98	6.68	5.15	-	-	-
	ZE41-3	2.1859	2.096	89.9	6.43	6.38	4.21	49.1	2.29	0.54

ACCEPTED MANUSCRIPT

	ZE41-4	2.3048	2.2147	90.1	6.63	6.53	4.11	52.45	2.34	0.58
	HP Mg-1	2.0484	2.038	10.4	7.5	7.43	0.42	-	-	-
	HP Mg-2	2.4934	2.4253	14.1	8.45	8.37	0.51	-	-	-
	HP Mg-3	1.7776	1.763	14.6	6.94	6.87	0.64	10	0.44	nm
	HP Mg-4	2.4985	2.4873	11.2	8.54	8.43	0.4	22	0.78	nm
	AZ91-1	3.0762	3.0677	8.5	9.02	8.98	0.29	-	-	-
7.4	AZ91-2	3.0353	3.0265	8.8	8.87	8.83	0.3	-	-	-
	AZ91-3	3.2853	3.2736	11.7	9.41	9.35	0.38	2.1	0.07	nm
	AZ91-4	3.5826	3.5705	12.1	10.09	10.6	0.36	1.8	0.05	nm
	ZE41-1	2.2894	2.215	74.4	7.92	7.87	2.86	-	-	-
	ZE41-2	1.98	1.8679	112.1	7.06	7.04	4.83	-	-	-
	ZE41-3	2.0756	2.0045	71.1	7.15	7.12	3.03	34.5	1.46	0.48
	ZE41-4	1.9455	1.8817	63.8	6.97	6.89	2.8	35.4	1.5	0.54
	HP Mg-1	2.6907	2.6813	9.4	8.74	8.67	0.33	-	-	-

ACCEPTED MANUSCRIPT

	HP Mg-2	2.346	2.337	9	8.12	8.03	0.34	-	-	-
	HP Mg-3	2.4263	2.4187	7.6	8.32	8.25	0.28	nm	-	-
	HP Mg-4	2.1581	2.1525	5.6	7.72	7.61	0.22	nm	-	-
8.2	AZ91-1	3.1589	3.1519	7	9.15	9.13	0.23	-	-	-
	AZ91-2	3.4424	3.436	6.4	9.65	9.61	0.2	-	-	-
	AZ91-3	3.173	3.1694	3.6	9.12	9.07	0.12	nm	-	-
	AZ91-4	3.1799	3.1761	3.8	9.2	9.17	0.13	nm	-	-
	ZE41-1	2.1919	2.1297	62.2	7.4	7.36	2.56	-	-	-
	ZE41-2	2.1961	2.1904	86.7	7.37	7.29	3.59	-	-	-
	ZE41-3	2.1145	2.043	71.5	7.33	7.27	2.97	36.2	1.48	0.5
	ZE41-4	1.7149	1.6443	70.6	6.47	6.41	3.33	32.5	1.51	0.45